

Light-Induced Currents at Domain Walls in Multiferroic BiFeO₃

Burak Guzelturk,^{*,†,‡,§} Antonio B. Mei,[§] Lei Zhang,^{||} Liang Z. Tan,[⊥] Patrick Donahue,^{||} Anisha G. Singh,[#] Darrell G. Schlom,[§] Lane W. Martin,^{||,⊙} and Aaron M. Lindenberg^{*,†,‡,∇,◇}

[†]Department of Materials Science and Engineering, Stanford University, Stanford, California 94305, United States

[‡]Stanford Institute for Materials and Energy Sciences, SLAC National Accelerator Laboratory, Menlo Park, California 94025, United States

[§]Department of Materials Science and Engineering and Kavli Institute at Cornell for Nanoscale Science, Cornell University, Ithaca, New York 14853, United States

^{||}Department of Materials Science and Engineering, University of California Berkeley, Berkeley, California 94720, United States

[⊥]Molecular Foundry and [⊙]Materials Sciences Division, Lawrence Berkeley National Laboratory, Berkeley, California 94720, United States

[#]Department of Applied Physics, Stanford University, Stanford, California 94305, United States

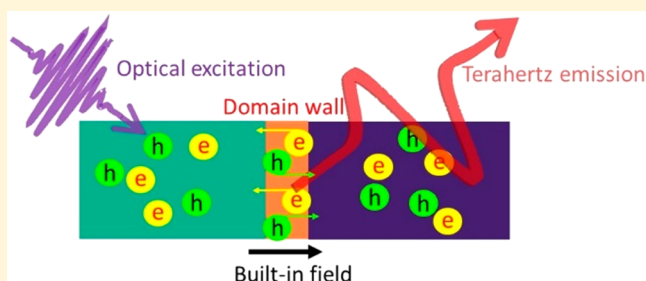
[∇]The PULSE Institute for Ultrafast Energy Science, SLAC National Accelerator Laboratory, Menlo Park, California 94025, United States

[◇]Department of Photon Science, Stanford University and SLAC National Accelerator Laboratory, Menlo Park, California 94025, United States

Supporting Information

ABSTRACT: Multiferroic BiFeO₃ (BFO) films with spontaneously formed periodic stripe domains can generate above-gap open circuit voltages under visible light illumination; nevertheless the underlying mechanism behind this intriguing optoelectronic response has not been understood to date. Here, we make contact-free measurements of light-induced currents in epitaxial BFO films via detecting terahertz radiation emanated by these currents, enabling a direct probe of the intrinsic charge separation mechanisms along with quantitative measurements of the current amplitudes and their directions. In the periodic stripe samples, we find that the net photocurrent is dominated by the charge separation across the domain walls, whereas in the monodomain samples the photovoltaic response arises from a bulk shift current associated with the non-centrosymmetry of the crystal. The peak current amplitude driven by the charge separation at the domain walls is found to be 2 orders of magnitude higher than the bulk shift current response, indicating the prominent role of domain walls acting as nanoscale junctions to efficiently separate photogenerated charges in the stripe domain BFO films. These findings show that domain-wall-engineered BFO thin films offer exciting prospects for ferroelectric-based optoelectronics, as well as bias-free strong terahertz emitters.

KEYWORDS: Ferroelectrics, BiFeO₃, domain walls, photovoltaic effect, shift current, terahertz emission



Today, materials that enable efficient solar energy harvesting are under intensive research.^{1–6} To this end, ferroelectrics have long attracted interest due to anomalous photovoltaic responses that were observed in prototypical systems such as LiNbO₃.^{7–9} Recently, thin films of multiferroic oxide BiFeO₃ (BFO) with spontaneously formed stripe domains exhibited such a response reflected by open circuit voltages that are much larger than the band gap of the material.^{10–12} This observation led to an ever-increasing interest in BFO thin films for a wide range of optoelectronic applications, but the underlying mechanism behind this anomalous response in the stripe domain BFO films has remained puzzling. Early reports identified the critical role of domain walls (DWs) in photovoltaic response as evidenced by

sample orientation dependent photovoltage measurements.^{10,11,13} In agreement with this, Seidel et al. proposed that photovoltages generated by the DWs are additive; hence photoresponse of the DWs underlies the observed above gap open circuit voltages.¹¹ Nevertheless, other reports suggested dominant contributions of the bulk photovoltaic effects^{12,14–16} inferred from excitation light polarization dependence of the measured photocurrents. Also, ref 12 indicated a potential detrimental role of the DWs in photovoltage generation due to

Received: August 23, 2019

Revised: November 13, 2019

Published: November 20, 2019

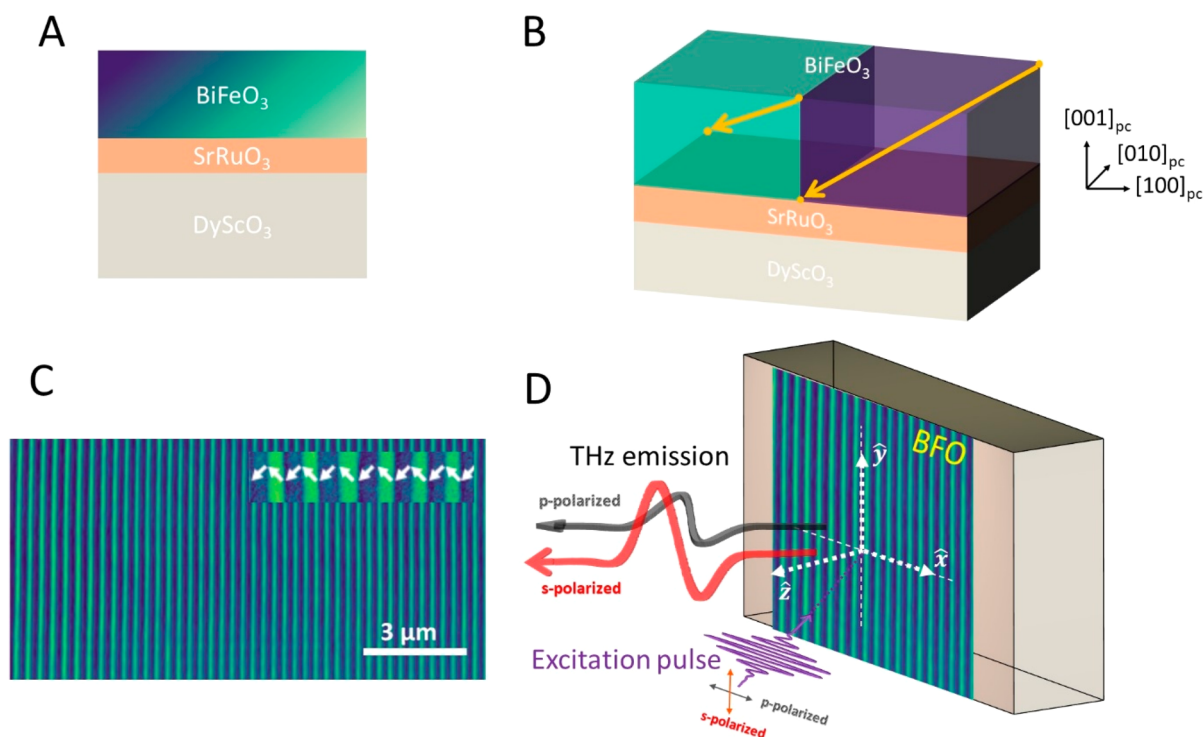


Figure 1. (a) Schematic shows film stack of the stripe domain BFO samples. (b) Spontaneous ferroelectric polarization direction (in-plane and out-of-plane) with respect to the crystal axes in the stripe domain samples with 71° domain walls. The samples exhibit net in-plane polarization along $[100]_{pc}$. (c) Piezoresponse force microscopy image of the periodic stripe domains. The inset shows the in-plane ferroelectric polarization components in two domain variants by white arrows. (d) Schematic shows the oblique incidence angle reflection configuration for the terahertz (THz) emission experiments. The emitted electromagnetic radiation is either p- or s-polarized. Crystal axes $[001]_{pc}$ and $[100]_{pc}$ point along \hat{z} and \hat{x} , respectively, and subscript pc denotes the pseudocubic notation for the BFO.

their large intrinsic conductivity, which opposed the DW-mediated photovoltaic mechanisms.¹¹ Therefore, the individual contributions of different photovoltaic mechanisms in BFO films have not been disentangled and remain debated to date.^{3,4,17}

A common complication in prior experimental studies was that optoelectronic characterization was typically performed using devices with physical electrodes, where metal–ferroelectric interfaces can greatly modify photovoltaic response due to the formation of Schottky barriers,^{18,19} field screening, and generation of interfacial defects.²⁰ For example, Pintilie et al. found that the photovoltaic response in ferroelectric $\text{Pb}(\text{Zr}, \text{Ti})\text{O}_3$ varies with the choice of metal used as the top contact.¹⁹ Although samples with Au and Ag contacts exhibited a bulk photovoltaic response, the ones using Pt and Cu exhibited a different one dominated by the band bending at the interface. This emphasizes the need for contact-free measurements of light-induced currents in photovoltaic ferroelectrics to extract and understand intrinsic physical phenomena. To this end, terahertz (THz) emission provides an all-optical means to measure light-induced currents, with the emitted fields directly arising from time-varying currents and their polarization state encoding the direction of the currents. This approach has been employed in prior studies to probe the initial steps of charge separation in semiconductor surfaces^{21–24} and photoinduced currents in spintronic²⁵ and topological²⁶ systems. Furthermore, state-of-the-art THz detection systems offer high sensitivity and can detect electromagnetic radiation emitted by transient currents arising from charge separation across sub-nanometer thick two-dimensional heterointerfaces.²⁷

Here, we report the observation of broadband terahertz radiation emitted by epitaxial BFO films in the absence of external bias or prior electrical poling. By analyzing the polarization properties of the emitted THz fields, we find that the light-induced currents in periodic stripe-domain BFO samples exclusively flow perpendicular to the DWs, which emerges due to the dominant charge separation at the domain walls. The DW-mediated current response is further confirmed by measurements as a function of domain-wall density, showing scaling with density. Samples with stripe domain structure grown via two different growth techniques also exhibit the same response; hence DW-mediated charge separation is intrinsic to the periodic stripe BFO films and independent of growth technique. In the case of monodomain BFO, measurements supported with first-principles modeling^{14,16} indicate that the light-induced currents follow a shift current response. Shift current is a bulk photovoltaic effect²⁸ that arises in non-centrosymmetric crystals when the evolution of excited electron and hole wave functions under a driving optical field is asymmetric^{29,30} and has been shown to boost photovoltaic performance in energy-relevant materials.^{31,32} We find that the DW-mediated peak photocurrent is 2 orders of magnitude stronger as compared to that of the bulk shift current response. Thus, DW-mediated charge separation in the periodic stripe BFO films is substantially more efficient than bulk photovoltaic effects in BFO at room temperature.

We investigate THz emission from stripe domain $\text{BiFeO}_3/\text{SrRuO}_3/\text{DyScO}_3$ (110)_O films (see Figure 1a) in a reflection geometry with an oblique incidence excitation (Figure 1d and Figure S1). The subscript O denotes the orthorhombic indices of the DyScO_3 substrate in the nonstandard $Pbmn$ setting;

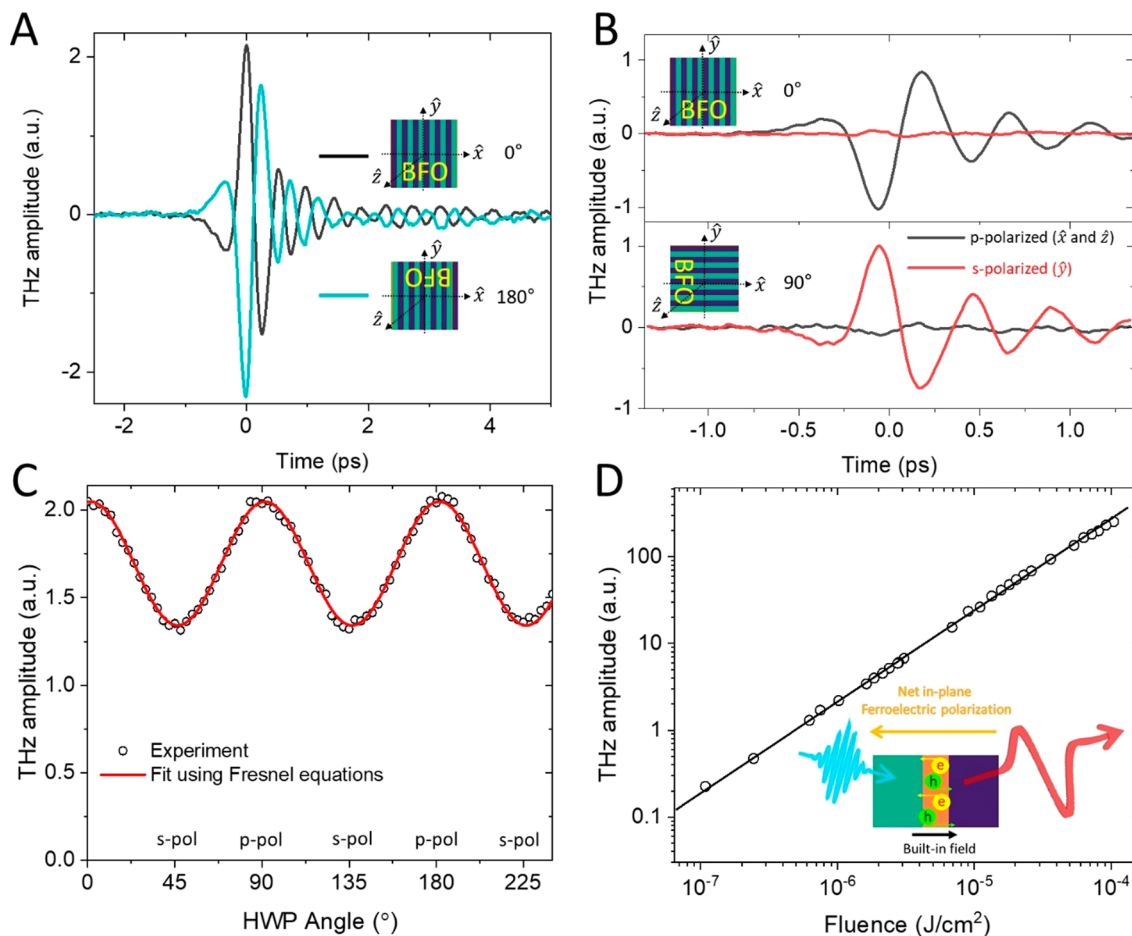


Figure 2. (a) Time-domain THz transients for the sample in 0° and 180° orientations, where 0° corresponds to the direction where DWs lie along \hat{y} . Detected THz fields are p-polarized. (b) Polarization-resolved THz transients for p- (black) and s-polarization (red) for the sample orientations of 0° (top) and 90° (bottom). (c) Excitation light polarization dependence of the THz emission (sample is oriented in 0°). The half wave plate (HWP) angle is varied while monitoring the peak THz amplitude. The fit is performed using the Fresnel equations to account for the polarization dependent reflection/transmission at the BFO surface. (d) Fluence dependence of the THz emission amplitude. The inset shows the THz emission mechanism in the periodic stripe domain sample, which arises due to efficient charge separation across the domain walls due to the built-in electric field at the domain walls.

these substrates are commonly used to achieve two domain variants in BiFeO₃ films separated by 71° domain walls.³³ In these samples, there exist both net in-plane and out-of-plane ferroelectric polarization (see Figure 1b). Figure 1c shows a piezo force microscopy image of the stripe domains with the inset showing the in-plane polarizations associated with two domain variants. Above-band gap 400 nm femtosecond pulses are used for excitation with the emitted THz fields, and their polarization states are detected using electro-optic sampling. Figure 2a shows the emitted THz transients measured for two different azimuthal orientations of the sample (0° and 180°). A 0° orientation means that the DWs lie along $+\hat{y}$, perpendicular to the xz plane of incidence of the 400 nm pulse and the net in-plane polarization points along $-\hat{x}$. When the sample is azimuthally rotated by 180°, the polarity of the THz field completely flips (Figure 2a). This indicates that the transient current giving rise to the emitted THz fields must be an in-plane current. The polarization state of the emitted THz field is further resolved with the help of two wire-grid THz polarizers (Figure S2). Figure 2b shows the THz transients measured for two orthogonal polarization states (p and s) when the sample is oriented 0° (top panel) and 90° (bottom panel). In both configurations, the radiated field is polarized

perpendicular to the DWs with a negligible contribution (<5%) parallel to the DWs. This observation indicates that the net current dominantly flows perpendicular to the DWs. Therefore, emission mechanisms such as surface band bending²¹ and photo-Dember²² effects, which would produce only net out-of-plane currents, can be ruled out. The absence of strong out-of-plane current despite the existence of net out-of-plane ferroelectric polarization implies that bulk photo-voltaic response (e.g., shift current¹⁶) is significantly weaker as compared to the DW-mediated currents. Importantly, we find the direction of the net in-plane current by comparing the emitted THz polarization to that of a well-known surface emitter (Figure S3). In the orientation of 0°, the net in-plane current flows along \hat{x} ; therefore, it flows antiparallel to the direction of the net in-plane ferroelectric polarization consistent with a screening response driven by the built-in fields at the DWs¹¹ where the built-in fields at the DWs are also antiparallel to the net in-plane ferroelectric polarization (see Figure 2d, inset, and Figure S7), agreeing with the prior predictions.¹¹

Figure 2c shows the excitation light polarization dependence of the emitted THz radiation. As the half wave plate (for 400 nm pump) is rotated, the THz amplitude oscillates with a DC

offset. This oscillatory behavior is completely captured by the Fresnel equations for an oblique incidence excitation considering the varying degree of reflection and transmission at the sample surface (Supporting Information). This observation further supports the argument that the bulk photovoltaic effect is not dominant in the periodic stripe BFO sample, since this effect²⁸ would have led to a strong dependence on the excitation light polarization in addition to the Fresnel coefficients, which will be discussed for the monodomain sample below.

Figure 2d shows the fluence dependence of the THz emission, where the radiated THz field is observed to increase linearly within a large range from 0.1 to 100 $\mu\text{J}/\text{cm}^2$. THz emission does not show saturation behavior within this range; thus charge separation at the DWs remains efficient even under high excitation density. It is important to note that an excitation fluence of 0.1 $\mu\text{J}/\text{cm}^2$ ($\sim 500 \text{ mW}/\text{cm}^2$) corresponds to a 5-sun-equivalent excitation (Supporting Information); hence the currents resolved here are of relevance to the photovoltaic operation. The radiated THz field amplitude (E_{THz}) can be related to its transient source current by assuming a sheet current density (J_{surface}):³⁴

$$E_{\text{THz}} = \eta J_{\text{surface}} Z_0 \quad (1)$$

where η is the outcoupling factor and Z_0 is the impedance of free space. We experimentally find $E_{\text{THz}} = 24.4 \text{ V/cm}$ under an excitation fluence of 30 $\mu\text{J}/\text{cm}^2$, and this field corresponds to an associated net J_{surface} of 40 A/m. Using J_{surface} , the areal coverage of the DWs ($\sim 1.5\%$), and the conductivity at THz range, we apply Ohm's law to estimate the built-in field (F_{DW}), which is 23.7 MV/m (see further details of the calculation in the Supporting Information). The built-in field agrees well with our estimate ($F_{\text{DW}} = 22 \text{ MV/m}$) using density functional theory for the 71° DWs (see Figure S7) and is in accordance with the previous theoretical prediction ($F_{\text{DW}} = 40 \text{ MV/m}$).¹¹ We further justify the built-in field at the DWs by considering a counter field that arises due to the screening of separated electron–hole pairs across a parallel plate: $E_{\text{rev}} = n/(\epsilon_0 \epsilon_r)$, where n is charge density across the DW. We estimate the counter field to be $E_{\text{rev}} = 24.1 \text{ MV/m}$ under a fluence of 100 $\mu\text{J}/\text{cm}^2$, where the emitted THz amplitude does not show a saturation (Figure 2d). Therefore, the built-in field F_{DW} must be equal to or larger than the E_{rev} , corroborating the F_{DW} estimated above. As compared to the conventional photoconductive THz emitters, which are typically biased with an acceleration field of a few MV/m, the DWs in BFO films with periodic stripe domains offer larger built-in acceleration fields at the nanoscale. Therefore, bias-free THz emitters based on stripe-domain BFO could offer comparable or even stronger THz amplitudes than those of state-of-the-art photoconductive THz emitters.³⁵ In comparison to conventional surface THz emitters (e.g., InSb), emitted THz amplitude from stripe domain BFO is smaller only by a factor of 4 under the same excitation condition. However, the domain walls only constitute $\sim 1.5\%$ of the BFO film; hence there is much room to boost THz emission further with samples having higher densities of DWs. Figure S4 also shows the spectrum of the emitted THz radiation from the stripe-domain samples, which has a bandwidth up to 7.5 THz that is limited by our electro-optic detection system. Therefore, bias-free THz emitters based on BFO films with periodic stripes could offer complete spectral coverage of the THz band (0.1–10 THz).

Figure 3 compares the THz field amplitudes emitted by three different periodic domain samples that were grown via

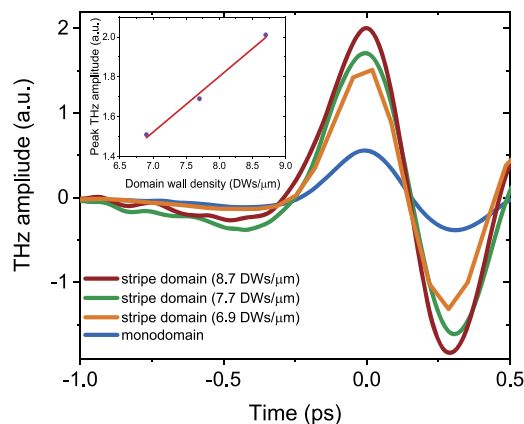


Figure 3. Radiated THz transients from three different stripe domain samples with 8.7 DWs/ μm (red), 7.7 DWs/ μm (green), and 6.9 DWs/ μm (orange), and monodomain BFO sample (blue) under the same excitation condition. All the samples are in the orientation of 0° as described in the text. The inset shows the peak THz amplitude as a function of DW density exhibiting a linear scaling.

two different methods (i.e., pulsed-laser deposition¹⁰ and molecular-beam epitaxy³⁶). All of the samples consistently exhibit the DW-mediated response described above. The DW densities of the samples are 8.7, 7.7, and 6.9 DWs/ μm (Figure S8 and Figure S9 for the PFM images of the samples) with thicknesses ranging from 70 to 220 nm. Importantly, increase in the DW density in stripe-domain BFO films leads to a larger THz field amplitude, and the peak THz amplitudes exhibit a linear scaling with DW density (see the inset of Figure 3) in good support of the DW-mediated charge separation mechanism. Furthermore, Figure 3 shows the THz emission from a 100 nm thick monodomain (untwinned) BFO ($\text{BiFeO}_3/\text{SrRuO}_3/\text{SrTiO}_3$) in $(110)_{\text{ps}}$ (in pseudocubic notation for the BFO), which has 3.5-fold smaller amplitude as compared to the samples with periodic stripe domains. All measurements in Figure 3 are done with the samples in the orientation of 0°, which will be defined for the monodomain sample in Figure 4. Also, to note, none of the samples were poled prior to the measurements.

Previously, THz emission was observed in monodomain BFO films that were electrically poled prior to the measurements.^{37,38} The THz emission, which was detected under surface normal excitation in a transmission geometry, was attributed to ultrafast depolarization of the ferroelectric polarization.³⁷ However, other potential mechanisms such as shift currents, which arise from a second order nonlinearity under above-gap excitation conditions in non-centrosymmetric BFO crystal,¹⁶ could not be ruled out since neither was excitation light polarization dependence investigated nor were out-of-plane currents probed. To elucidate the emission mechanism in the monodomain BFO, THz transients are measured for different azimuthal orientations of the sample (0°, 90°, 180°, and 270°) with the pump polarization first fixed as p-polarized (Figure 4a). Figure 4b depicts the ferroelectric polarization in the monodomain sample exhibiting net in-plane and out-of-plane polarizations with respect to the crystal axes. Figure 4c shows the ferroelectric polarization directions under different sample orientations. The electro-optic sampling

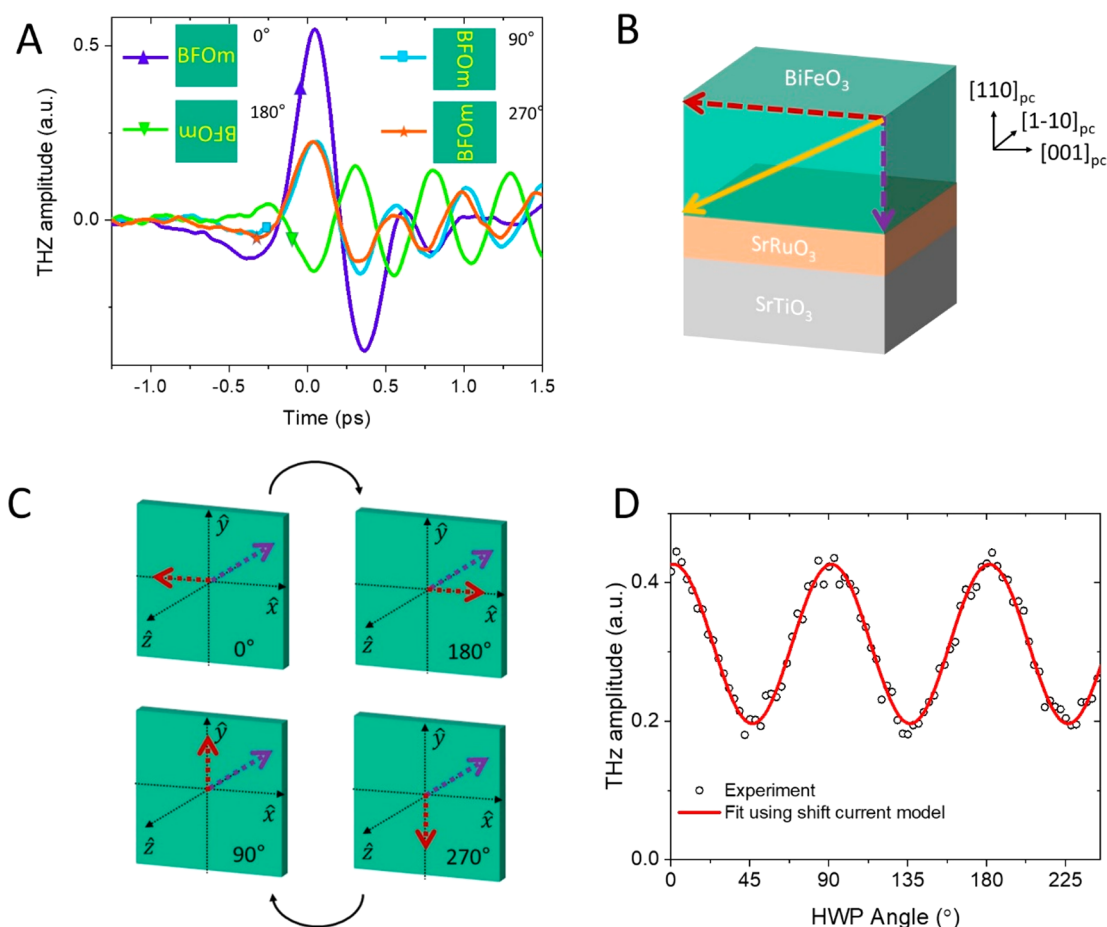


Figure 4. (a) Radiated THz transients for different azimuthal orientations of the monodomain (110) BFO sample. (b) Ferroelectric polarization with respect to the crystal axes in the monodomain BFO thin film. The in-plane and out-of-plane components are marked by red and purple arrows, respectively. (c) Depiction of the in-plane (red) and out-of-plane (purple) ferroelectric polarizations for different azimuthal orientations of the monodomain sample. Crystal axes $[110]_{pc}$ and $[001]_{pc}$ point along \hat{z} and \hat{x} , respectively. (d) Excitation light polarization dependence (half wave plate, HWP) of the emitted THz radiation from the monodomain BFO. The fit is performed using the shift current model described in the Supporting Information.

system is fixed such that it is only sensitive for p-polarized THz radiation; therefore, we resolve net currents that flow along \hat{x} or \hat{z} . Sample orientations of 90° and 270° exhibit the same signal amplitude without a polarity flip, which implies that the net current giving rise to the detected p-polarized THz emission in these orientations must be only out-of-plane. On the other hand, the orientations of 0° and 180° exhibit a polarity reversal, with 0° orientation exhibiting larger absolute amplitude than that of 180°. This observation can be explained with the coexistence of in-plane (\hat{x}) and out-of-plane (\hat{z}) currents projecting together onto a p-polarized emission, where the currents are additive for the orientation of 0° but subtractive for the 180° orientation (see Figure 4c). By comparing the THz amplitudes measured under 0° and 180° orientations, we find that 65% (35%) of the THz emission stems from the in-plane (out-of-plane) currents in the orientation of 0°. Moreover, in the 0° orientation net in-plane and out-of-plane currents point along \hat{x} and \hat{z} , respectively. Therefore, photocurrents (in-plane and out-of-plane) flow antiparallel to the intrinsic ferroelectric polarizations as prior studies suggested,³⁸ but the underlying mechanism requires detailed investigation of the excitation light polarization dependence. Figure 4d shows the excitation light polarization dependence of the emitted THz amplitude

for the monodomain sample that is orientated at 90° (the same for 270°), where the detected p-polarized THz emission arises only from an out-of-plane current. The modulation of the THz amplitude as a function of the half-wave plate angle cannot be captured by any means considering the Fresnel equations alone (see Figure S10), which signifies that the emission is not directly associated with the density of photogenerated carriers. Therefore, this rules out the ultrafast depolarization of the ferroelectric polarization as a mechanism for the THz emission here, which would only depend on the density of carriers created. To account for the excitation light polarization dependence, we theoretically estimate the shift currents by considering the shift current tensor under 400 nm optical excitation for varying excitation polarization, and Figure S6 shows the predicted nonlinear conductivity for the in- and out-of-plane shift current components. As shown in Figure 4d, the out-of-plane shift current ($J_{[110]}^{\text{shift}}$) excellently fits the excitation polarization dependence of the detected p-polarized THz emission under the orientation of 90°, for both the modulation depth and the phase without any additional fit parameter needed. This observation strongly indicates that the THz emission in the monodomain BFO arises from a shift current response.

Moreover, we compare the amplitudes of the transient currents in the monodomain BFO and the calculated shift currents. The experimental J_{surface} in the monodomain sample is calculated to be 9 and 16 A/m for the in-plane and out-of-plane currents, respectively. The out-of-plane current amplitude is larger than that of the in-plane one but the emitted THz by the in-plane current is stronger since the outcoupling coefficient (η) associated with the in-plane current is larger by a factor of 4. The experimental currents in the monodomain sample are in excellent agreement with our theoretical estimates of the shift current densities, which are 10.3 and 13.3 A/m for the in-plane and out-of-plane components, respectively (see Supporting Information for the details of the calculation). The consistency between the experimental current amplitudes and the first principle calculations shows additional strong evidence that the photovoltaic effect in the monodomain BFO is governed by the shift current response.

To compare the bulk shift current amplitudes to the DW-mediated currents, we consider the spatially localized nature of the currents associated with the DWs, and we estimate the peak DW-mediated current amplitude as $J_{\text{DW}} = 40 \frac{\text{Å}}{\text{m}} \times \frac{1}{1.5\%} = 2670 \text{ A/m}$, where 1.5% comes from the areal coverage of the DWs. Therefore, the current density associated with the charge separation at the DWs is more than 2 orders of magnitude larger as compared to the bulk shift current response. This further highlights the importance of DWs providing nanoscale junctions for efficient charge separation. Therefore, periodic domain walls act as series connected voltage sources at the nanoscale, which underpins the unique optoelectronic functionality observed in these photoferroic thin films.¹⁰

In summary, we disentangle and quantify the unique contributions of different photovoltaic mechanisms in epitaxial BFO films. In BFO with periodic stripe domains, domain-wall-mediated charge separation is found to be the dominant mechanism, whereas a shift current response dominates in the case of monodomain BFO. We show that light-induced currents are significantly stronger in BFO with stripe domains as compared to monodomain BFO due to the dominance of the domain-wall-mediated currents over the shift current response. Overall, BFO films with spontaneously formed periodic stripes offer exciting prospects as bias-free THz emitters. Control of the domain wall density could enable practical broadband THz emitters based on ferroelectric materials.

■ ASSOCIATED CONTENT

Supporting Information

The Supporting Information is available free of charge at <https://pubs.acs.org/doi/10.1021/acs.nanolett.9b03484>.

THz emission spectroscopy setup, polarization analysis of the emitted THz radiation, calibration of the current directions, calculation of the peak THz field amplitude, calculation of the built-in fields at the domain walls, shift current calculations, piezo force microscopy images of the samples, and growth procedures of the samples (PDF)

■ AUTHOR INFORMATION

Corresponding Authors

*Email: burakg@stanford.edu.

*Email: aaronl@stanford.edu.

ORCID

Burak Guzelturk: 0000-0003-1977-6485

Lei Zhang: 0000-0002-1559-8469

Liang Z. Tan: 0000-0003-4724-6369

Lane W. Martin: 0000-0003-1889-2513

Aaron M. Lindenberg: 0000-0003-3233-7161

Notes

The authors declare no competing financial interest.

■ ACKNOWLEDGMENTS

The terahertz spectroscopy work was supported by the Department of Energy, Basic Energy Sciences, Materials Sciences and Engineering Division. L.Z. acknowledges support from the Army Research Office under Grant W911NF-14-1-0104. P.D. acknowledges support from the National Science Foundation under Grant DMR-1708615. L.W.M. and A.M.L. acknowledge support from the U.S. Department of Energy, Office of Science, Office of Basic Energy Sciences, under Award Number DE-SC-0012375 for the study of ultrafast response of ferroic materials. A.B.M. and D.G.S. acknowledge support from the Semiconductor Research Corporation (SRC) as nCORE task No. 2758.003 and the National Science Foundation (NSF) under the E2CDA (Grant No. ECCS 1740136) programs. Substrate preparation was performed in part at the Cornell NanoScale Facility, a member of the National Nanotechnology Coordinated Infrastructure (NNCI), which is supported by the NSF (Grant No. ECCS-1542081). L.Z.T. was supported by the Molecular Foundry at Lawrence Berkeley National Laboratory, supported by the Office of Science, Office of Basic Energy Sciences, of the US Department of Energy under Contract No. DE-AC02-05CH11231. The authors would like to thank Dr. Xiaojun Wu for useful discussion on characterization of THz polarization states.

■ REFERENCES

- (1) *Ferroelectric materials for energy applications*; Huang, H., Scott, J. F., Eds.; Wiley-VCH Verlag, 2018.
- (2) Martin, L. W.; Rappe, A. M. *Nat. Rev. Mater.* **2017**, 2 (2), 16087.
- (3) Paillard, C.; Bai, X.; Infante, I. C.; Guennou, M.; Geneste, G.; Alexe, M.; Kreisel, J.; Dkhil, B. *Adv. Mater.* **2016**, 28 (26), 5153–5168.
- (4) Fan, Z.; Sun, K.; Wang, J. *J. Mater. Chem. A* **2015**, 3 (37), 18809–18828.
- (5) Kreisel, J.; Alexe, M.; Thomas, P. A. *Nat. Mater.* **2012**, 11 (4), 260–260.
- (6) Seidel, J. *Nat. Mater.* **2019**, 18 (3), 188–190.
- (7) Glass, A. M.; von der Linde, D.; Negran, T. J. *Appl. Phys. Lett.* **1974**, 25 (4), 233–235.
- (8) Sturman, B. I.; Fridkin, V. M. *The photovoltaic and photorefractive effects in noncentrosymmetric materials*; Gordon and Breach Science Publishers, 1992.
- (9) Agarwal, R.; Sharma, Y.; Chang, S.; Pitike, K. C.; Sohn, C.; Nakhmanson, S. M.; Takoudis, C. G.; Lee, H. N.; Tonelli, R.; Gardner, J.; Scott, J. F.; Katiyar, R. S.; Hong, S. *Phys. Rev. B: Condens. Matter Mater. Phys.* **2018**, 97 (5), 054109.
- (10) Yang, S. Y.; Seidel, J.; Byrnes, S. J.; Shafer, P.; Yang, C.-H.; Rossell, M. D.; Yu, P.; Chu, Y.-H.; Scott, J. F.; Ager, J. W.; Martin, L. W.; Ramesh, R. *Nat. Nanotechnol.* **2010**, 5 (2), 143–147.
- (11) Seidel, J.; Fu, D.; Yang, S.-Y.; Alarcón-Lladó, E.; Wu, J.; Ramesh, R.; Ager, J. W. *Phys. Rev. Lett.* **2011**, 107 (12), 126805.
- (12) Bhatnagar, A.; Roy Chaudhuri, A.; Heon Kim, Y.; Hesse, D.; Alexe, M. *Nat. Commun.* **2013**, 4 (1), 2835.

- (13) Matsuo, H.; Kitanaka, Y.; Inoue, R.; Noguchi, Y.; Miyayama, M.; Kiguchi, T.; Konno, T. *J. Phys. Rev. B: Condens. Matter Mater. Phys.* **2016**, *94* (21), 214111.
- (14) Ji, W.; Yao, K.; Liang, Y. C. *Phys. Rev. B: Condens. Matter Mater. Phys.* **2011**, *84* (9), 094115.
- (15) Yan, F.; Chen, G.; Lu, L.; Spanier, J. E. *ACS Nano* **2012**, *6* (3), 2353–2360.
- (16) Young, S. M.; Zheng, F.; Rappe, A. M. *Phys. Rev. Lett.* **2012**, *109* (23), 236601.
- (17) Butler, K. T.; Frost, J. M.; Walsh, A. *Energy Environ. Sci.* **2015**, *8* (3), 838–848.
- (18) Pintilie, L.; Alexe, M. J. *J. Appl. Phys.* **2005**, *98* (12), 124103.
- (19) Pintilie, L.; Dragoi, C.; Pintilie, I. *J. Appl. Phys.* **2011**, *110* (4), 044105.
- (20) Lee, D.; Baek, S. H.; Kim, T. H.; Yoon, J.-G.; Folkman, C. M.; Eom, C. B.; Noh, T. W. *Phys. Rev. B: Condens. Matter Mater. Phys.* **2011**, *84* (12), 125305.
- (21) Zhang, X.-C.; Hu, B. B.; Darrow, J. T.; Auston, D. H. *Appl. Phys. Lett.* **1990**, *56* (11), 1011–1013.
- (22) Gu, P.; Tani, M. In *Terahertz Optoelectronics*; Springer-Verlag: Berlin/Heidelberg, 2005; pp 63–98.
- (23) Guzelturk, B.; Belisle, R. A.; Smith, M. D.; Bruening, K.; Prasanna, R.; Yuan, Y.; Gopalan, V.; Tassone, C. J.; Karunadasa, H. I.; McGehee, M. D.; Lindenberg, A. M. *Adv. Mater.* **2018**, *30* (11), 1704737.
- (24) Schmuttenmaer, C. A. *Chem. Rev.* **2004**, *104* (4), 1759–1780.
- (25) Seifert, T.; Jaiswal, S.; Martens, U.; Hannegan, J.; Braun, L.; Maldonado, P.; Freimuth, F.; Kronenberg, A.; Henrizi, J.; Radu, I.; Beaupaire, E.; Mokrousov, Y.; Oppeneer, P. M.; Jourdan, M.; Jakob, G.; Turchinovich, D.; Hayden, L. M.; Wolf, M.; Münzenberg, M.; Kläui, M.; Kampfrath, T. *Nat. Photonics* **2016**, *10* (7), 483–488.
- (26) Sirica, N.; Tobey, R. I.; Zhao, L. X.; Chen, G. F.; Xu, B.; Yang, R.; Shen, B.; Yarotski, D. A.; Bownan, P.; Trugman, S. A.; Zhu, J.-X.; Dai, Y. M.; Azad, A. K.; Ni, N.; Qiu, X. G.; Taylor, A. J.; Prasankumar, R. P. *Phys. Rev. Lett.* **2019**, *122* (19), 197401.
- (27) Ma, E. Y.; Guzelturk, B.; Li, G.; Cao, L.; Shen, Z.-X.; Lindenberg, A. M.; Heinz, T. F. *Sci. Adv.* **2019**, *5* (2), No. eaau0073.
- (28) Belinicher, V. I.; Sturman, B. I. *Sov. Phys. Uspekhi* **1980**, *23* (3), 199–223.
- (29) Tan, L. Z.; Zheng, F.; Young, S. M.; Wang, F.; Liu, S.; Rappe, A. M. *npj Comput. Mater.* **2016**, *2* (1), 16026.
- (30) Sipe, J. E.; Shkrebtii, A. I. *Phys. Rev. B: Condens. Matter Mater. Phys.* **2000**, *61* (8), 5337–5352.
- (31) Cook, A. M.; M. Fregoso, B.; de Juan, F.; Coh, S.; Moore, J. E. *Nat. Commun.* **2017**, *8* (1), 14176.
- (32) Rangel, T.; Fregoso, B. M.; Mendoza, B. S.; Morimoto, T.; Moore, J. E.; Neaton, J. B. *Phys. Rev. Lett.* **2017**, *119* (6), 067402.
- (33) Chu, Y.-H.; He, Q.; Yang, C.-H.; Yu, P.; Martin, L. W.; Shafer, P.; Ramesh, R. *Nano Lett.* **2009**, *9* (4), 1726–1730.
- (34) Shan, J.; Heinz, T. F. In *Ultrafast Dynamical Processes in Semiconductors*; Springer: Berlin Heidelberg, 2004; pp 1–56.
- (35) Beck, M.; Schäfer, H.; Klatt, G.; Demsar, J.; Winnerl, S.; Helm, M.; Dekorsy, T. *Opt. Express* **2010**, *18* (9), 9251.
- (36) Mei, A. B.; Tang, Y.; Schubert, J.; Jena, D.; Xing, H. G.; Ralph, D. C.; Schlom, D. G. *APL Mater.* **2019**, *7* (7), 071101.
- (37) Takahashi, K.; Kida, N.; Tonouchi, M. *Phys. Rev. Lett.* **2006**, *96* (11), 117402.
- (38) Rana, D. S.; Kawayama, I.; Mavani, K.; Takahashi, K.; Murakami, H.; Tonouchi, M. *Adv. Mater.* **2009**, *21* (28), 2881–2885.